molecular pharmaceutics

pubs.acs.org/molecularpharmaceutics

Article

Dual-Targeted Radionuclide Therapy with ^{161}Tb Instigates Anticancer Immunity in "Cold" Murine Prostate Tumor

Juan Sun,[§] Jiakun Guo,[§] Xunhao Qi,[§] Jiangtao Yang, Guanglin Wang,* Guangming Zhou, Fenghua Meng, and Zhiyuan Zhong*

Cite This: *Mol. Pharmaceutics* 2026, 23, 4311−4321

Read Online

ACCESS | Metrics & More | Article Recommendations | Supporting Information

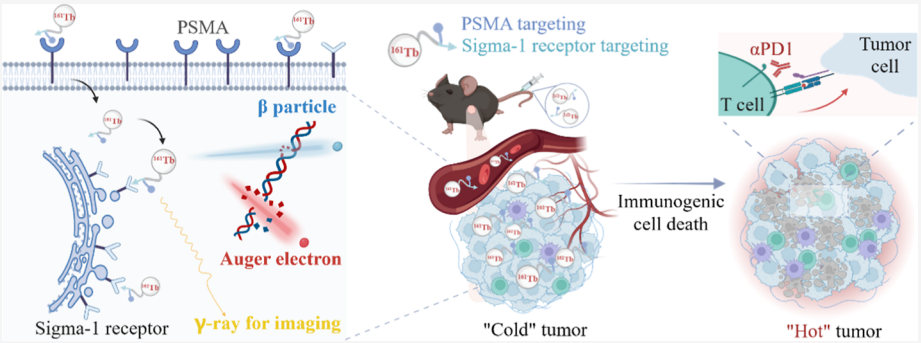

ABSTRACT: Targeted radionuclide therapy (TRT) with ^{177}Lu holds a huge clinical success in treating advanced prostate cancer patients. It is noted, however, that ^{177}Lu with moderate radiation energy achieves effective tumor inhibition at a relatively high dose and has a low capacity to activate "cold" prostate tumor. In this study, we report that Sigma-1 receptor and prostate-specific membrane antigen (PSMA) dual-targeted peptide (S1R/PSMA-P) labeled with ^{161}Tb, which emits locally high linear energy transfer (LET) Auger electrons, effectively inhibits prostate tumor and energizes anticancer immunity. ^{161}Tb−S1R/PSMA-P exhibited significantly enhanced cytotoxicity and immunogenic cell death over ^{177}Lu-labeled counterpart by inducing more DNA double-strand breaks and reactive oxygen species. Of note, ^{161}Tb−S1R/PSMA-P achieved high tumor uptake and selectivity, induced a complete regression rate of 60% at a single dose of 7.4 MBq in RM1-PSMA$^+$/RM1 tumor model, and sensitized RM1-PSMA$^+$/RM1 tumor to αPD1 immune checkpoint blockade therapy at a dose of 3.7 MBq resulting in a cure rate of 50% and durable antitumor immunity. Overall, ^{161}Tb−S1R/PSMA-P emerges as a promising theranostic agent that is capable of mitigating prostate tumor by boosting anticancer immunity.

KEYWORDS: *prostate cancer, targeted radionuclide therapy, beta particles, anticancer immunity, immune checkpoint blockade therapy*

1. INTRODUCTION

Targeted radionuclide therapy (TRT) has emerged as a transformative modality in cancer treatment, enabling precise tumor visualization, dosimetry-guided treatment planning and longitudinal therapeutic monitoring.[1−4] By delivering cytotoxic radiation selectively via tumor-specific ligand, TRT maximizes tumor damage while sparing healthy tissues.[5−7] However, the efficacy of TRT hinges critically on the physical properties of the radionuclide and the biological targeting strategy employed.

Beta (β^-)-emitters, such as ^{177}Lu, remain a cornerstone of clinical practice, highlighted by the clinical success and Food and Drug Administration approvals of ^{177}Lu-DOTATATE for neuroendocrine tumors and ^{177}Lu-PSMA-617 for metastatic castration-resistant prostate cancer.[8,9] However, the electrons emitted by ^{177}Lu with relatively low linear energy transfer (LET) often induces sublethal DNA damage that fosters radioresistance and provides insufficient cytotoxicity for micrometastases eradication.[10−12] The alpha (α)-emitters produce high LET radiation capable of causing irreparable DNA double-strand breaks.[13,14] Their clinical translation is, however, often hindered by limited availability, high cost, and narrow therapeutic windows.[15] ^{161}Tb represents a compelling alternative that bridges the gap between β^- therapy and α therapy. Chemically analogous to ^{177}Lu, ^{161}Tb emits not only medium-energy β^- particles but also abundant short-range, locally high LET Auger electrons.[16−18] These radiations confer a superior dosimetric profile. Monte Carlo simulations indicate that the absorbed dose from ^{161}Tb is 2.6−3.6× higher in

Received: May 10, 2026
Revised: June 27, 2026
Accepted: June 29, 2026
Published: July 3, 2026

Scheme 1. ^{161}Tb Radiolabeled Sigma-1 Receptor and PSMA Dual-Targeted Radioligand (^{161}Tb−S1R/PSMA-P) Mitigates Prostate Cancer and Boosts ICB Therapy[a]

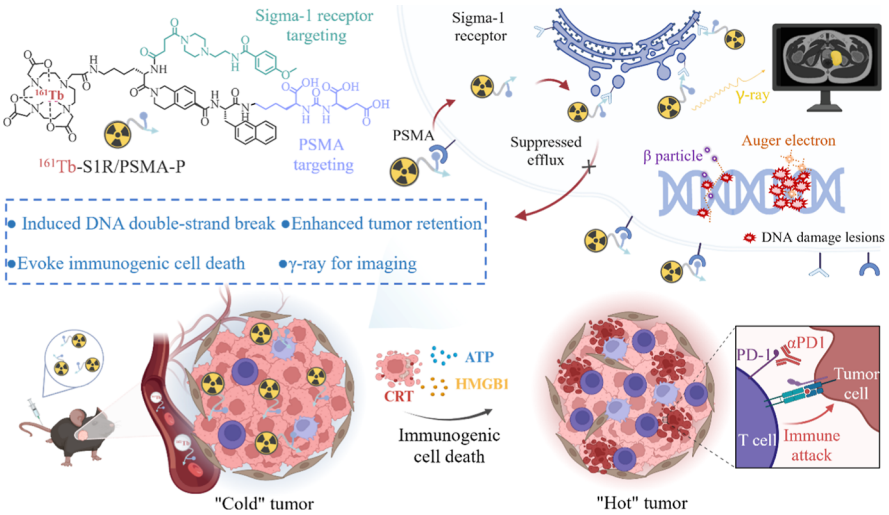

[a]^{161}Tb−S1R/PSMA-P achieves superior tumor inhibition due to the additional emission of Auger electrons from ^{161}Tb compared to its ^{177}Lu-labeled counterpart. ^{161}Tb−S1R/PSMA-P at a low dose is capable of boosting ICB therapy of "cold" murine prostate tumor.

single-cell models and 2.1−3.0× higher in the cell clusters than with ^{177}Lu.[19] This enhanced local energy deposition positions ^{161}Tb as a promising candidate to surpass the therapeutic efficacy of ^{177}Lu.

The immunomodulatory effects of TRT are gaining recognition for overcoming resistance to immune checkpoint blockade (ICB) in immunologically "cold" prostate tumors.[20,21] TRT counteracts this by inducing immunogenic cell death (ICD), whereby radiation triggers the release of tumor-associated antigens and damage-associated molecular patterns (DAMPs).[22,23] However, the immunological consequences depend heavily on radionuclides, ligand, and dosing and time of radiopharmaceuticals. Conventional low LET β^--emitters (e.g., ^{177}Lu) primarily expand existing adaptive immunity, often failing to inflame "cold" tumors, whereas high LET α-emitters initiate robust immune priming.[24] The immunomodulatory potential of ^{161}Tb is rarely investigated. We hypothesized that ^{161}Tb could elicit a more potent ICD response than conventional β^--emitters, offering an alternative strategy to sensitize prostate cancer to immunotherapy.

The efficacy of TRT highly depends on the ligand, for which various approaches such as albumin binding, covalent binding, multimerization, and dual-targeted strategies, have been investigated to improve its pharmacokinetics, and affinity to the target.[25−27] We recently developed an extracellular-intracellular dual-targeted peptide (S1R/PSMA-P) that following PSMA-mediated endocytosis binds to Sigma-1 receptors in the endoplasmic reticulum, effectively inhibiting drug efflux.[28,29] When radiolabeled with either ^{177}Lu or ^{225}Ac, this ligand demonstrated superior tumor uptake and retention, as well as enhanced efficacy in LNCaP prostate tumor xenografts compared to PSMA-617 control. This enhanced intracellular accumulation is particularly critical for ^{161}Tb, as its high LET Auger electrons have a short tissue penetration range and require close proximity to nuclear to exert maximal cytotoxicity. Herein, we leverage this dual-targeted platform S1R/PSMA-P to label ^{161}Tb and investigate its in vitro and in vivo toxicity as well as ability to boost immune checkpoint blockade (ICB) therapy in a "cold" murine prostate cancer model (Scheme 1). The results show that ^{161}Tb−S1R/PSMA-P achieved a complete regression rate of 60% at a single dose of 7.4 MBq in RM1-PSMA$^+$/RM1 tumor in mice, and effectively boosted the immune response to αPD1 therapy at a lower dose of 3.7 MBq. ^{161}Tb−S1R/PSMA-P has appeared as a promising radiopharmaceutics for the treatment of advanced prostate cancer.

2. EXPERIMENTAL SECTION

2.1. Materials

PSMA-617 was purchased from Topscience Co. Ltd. S1R/PSMA-P was kindly provided by Suzhou Ruihe Pharmaceutical Technology Co., Ltd. $^{161}TbCl_3$ and $^{177}LuCl_3$ were purchased from Chengdu Syncor Pharmaceutical Co., Ltd. (Chengdu, China). All other chemicals were used as received.

2.2. Radiosynthesis and Radiostability Test

Radiolabeling with both ^{177}Lu and ^{161}Tb was performed using identical reaction conditions based on previously established protocols.[30] Briefly, S1R/PSMA-P was dissolved in sodium ascorbate (0.4 M, pH 4.5) to a final concentration of 0.2 μg/μL. 37 MBq of $^{161}TbCl_3$ or $^{177}LuCl_3$ was mixed with 0.5 μg of ligand and adjusted to a total volume of 50 μL with sodium ascorbate (0.4 M, pH 4.5). The mixture was then heated at 95 °C for 15 min. The radiochemical yield (RCY) was determined by radio-TLC analysis (Lablogic, Scan-RAM) using a mobile phase of 1% EDTA 2Na. The radiostability of radioligands was assessed by radio-TLC after incubation with 10% fetal bovine serum (FBS) or phosphate-buffered saline (PBS) for 24, 48, 72, 96, 144, and 168 h.

2.3. In Vitro PSMA-Binding Assay

The RM1-PSMA$^+$ cells were constructed as previously reported[29,31] and cultured in DMEM (Basalmedia) containing 10% FBS (Gibco) at 37 °C in a 5% CO_2 atmosphere. RM1-PSMA$^+$ cells were seeded at a density of 5 × 10^4 cells/well in 24-well plates, and then incubated with ^{161}Tb−S1R/PSMA-P (37 kBq) or ^{177}Lu−S1R/PSMA-P (37 kBq) for 1, 4, and 24 h. Thereafter, the cells were washed with PBS, and membrane−bound activity was stripped with glycine buffer (50 mM glycine and 100 mM NaCl, pH 3), while internalized activity was collected by lysis with 1 M NaOH. The quantification of radioactivity was conducted using a gamma counter (PerkinElmer, Wallac 2480).

https://doi.org/10.1021/acs.molpharmaceut.6c00650
Mol. Pharmaceutics 2026, 23, 4311−4321

2.4. In Vitro Antitumor Assay

The assessment of cell viability was conducted through the implementation of the 3-(4,5-dimethylthiazol-2-yl)-2,5-diphenyltetrazolium bromide (MTT) assay, as previously described.[32] Briefly, RM1-PSMA$^+$ cells were seeded in 96-well plates (1×10^3/well, 80 μL) and cultured for 12 h. Following the addition of 20 μL of ^{161}Tb−S1R/PSMA-P and ^{177}Lu−S1R/PSMA-P at activity ranging from 0.01 to 1 MBq/mL, the cells were incubated for 48 h. Thereafter, 10 μL of MTT solution (5 mg/mL) was added for 4 h and the resultant data were quantified with a microplate reader at 570 nm. The cell viability was determined by comparing the absorbance of the cells treated with PBS.

For colony formation assay, RM1-PSMA$^+$ cells were seeded on 6-well plates (5×10^2/well) and left to grow overnight. The cells were then exposed to ^{161}Tb−S1R/PSMA-P and ^{177}Lu−S1R/PSMA-P (0.1 MBq/mL, 2 mL) for 48 h. Thereafter, the media was removed, and the cells were washed and permitted to proliferate into colonies over a five-day period. The colonies were fixed and stained with crystal violet and photographed.

The study of the DNA damage induced in RM1-PSMA$^+$ by radioligands was conducted by seeding RM1-PSMA$^+$ cells on 12 mm glass coverslips in 12-well plates (2×10^4/well) overnight, and subsequently treating them with ^{161}Tb−S1R/PSMA-P and ^{177}Lu−S1R/PSMA-P (0.1 MBq/mL) for 48 h. Following fixation with 4% paraformaldehyde at room temperature for 10 min, the cells were incubated with a primary antibody against γH2AX at 4 °C for 1 h, and then stained with Alexa Fluor 647-conjugated secondary antibodies at 4 °C for 30 min. The stained cells were mounted on a slide and imaged via confocal microscopy.

In order to examine the generation of reactive oxygen species (ROS), RM1-PSMA$^+$ cells were seeded on 12-well plates and left to grow overnight. The cells were then treated with ^{161}Tb−S1R/PSMA-P and ^{177}Lu−S1R/PSMA-P (0.1 MBq/mL, 1 mL) for a period of 48 h. Following this incubation period, the cells were stained with 10 μM DCFH-DA for the purpose of measuring the levels of ROS using flow cytometry.

2.5. Biodistribution Study

All animal experiments were approved by the Animal Care and Use Committee of Soochow University and conducted according to the Guidelines for the Care and Use of Experimental Animals (Ethics Approval Number: 202503A0856). The male C57BL/6 mice (6 weeks, 20−22 g) were procured from GemPharmatech Co., Ltd. and maintained under standard conditions. A mixture of RM1-PSMA$^+$ cells (4.5×10^6 cells) and RM1 cells (5×10^5 cells) was suspended in 100 μL of PBS and Matrigel (Corning, Arizona) at a 1:1 ratio and subcutaneously injected into the right flank of each mouse. Pure RM1-PSMA$^+$ tumors frequently underwent spontaneous shrinkage and occasional complete regression, likely due to the immunogenicity of exogenously expressed PSMA. Therefore, RM1 cells were mixed with RM1-PSMA$^+$ cells to establish a more stable tumor model that also better reflects the heterogeneous PSMA expression observed in clinical prostate cancer. When the tumors grew to approximately 100−200 mm^3, RM1-PSMA$^+$/RM1 tumor-bearing mice were used for microSPECT/CT imaging (Milabs, The Netherlands). Mice were intravenously administered ^{161}Tb−S1R/PSMA-P (11.1 MBq), ^{177}Lu−S1R/PSMA-P (11.1 MBq), or ^{161}Tb-PSMA-617 (11.1 MBq) via tail vein and then scanned at 1, 4, 8, 24, 48, 72, and 96 h postinjection (n = 3). The scanned data were then reconstructed using U-SPECT-Rec2.51g software and analyzed with PMOD software (Version 3.602).

In order to study pharmacokinetics, a group of healthy C57BL/6 mice was administered with radioligands (5.5 MBq) via intravenous injection. Blood samples were collected from the orbital plexus at 1, 5, 10, 15, 30 min, 1, 2, 4, 8, 24, 48, and 72 h (n = 3). The samples were weighed, and their radioactivity was measured using the gamma counter. The data underwent a process of decay correction prior to presentation as the percentage of the injected dose per gram of tissue (% ID/g).

2.6. In Vivo Therapy

In order to evaluate the therapy efficacy of the radioligand therapy, RM1-PSMA$^+$/RM1 tumor-bearing mice were divided into five groups at random and intravenously injected with PBS, ^{177}Lu−S1R/PSMA-P (7.4 MBq), ^{161}Tb-PSMA-617 (7.4 MBq), ^{161}Tb−S1R/PSMA-P (3.7 MBq), or ^{161}Tb−S1R/PSMA-P (7.4 MBq) (n = 6). Treatment was initiated on day 4 after tumor inoculation, when tumors had reached approximately 100−200 mm^3, exhibited a firm morphology, and showed substantial radioligand uptake by SPECT imaging. Tumor volume and body weight were measured on a twice−weekly basis. The volume of tumor (mm^3) was calculated using the following formula: 0.5 × length × width.[2] On the seventh day, a random selection of one mouse from each group was euthanized. The tumors were sectioned and subjected to staining for K_i-67, γ-H2AX, and hematoxylin and eosin (H&E). The toxicity of ^{161}Tb−S1R/PSMA-P was subsequently assessed in healthy mice at the dose of 14.8 and 29.6 MBq. Body weight was measured two occasions per week. On the 27th day, the mice were euthanized, and blood samples were collected for routine blood analysis and liver and kidney function tests. The major organs, including the heart, liver, spleen, lung, and kidney, were collected and sliced for analysis. The analysis was conducted using H&E staining.

In order to assess the ability of ^{161}Tb−S1R/PSMA-P to induce ICD in RM1-PSMA$^+$ cells, the expression of calreticulin (CRT), adenosine triphosphate (ATP), and high mobility group box 1 (HMGB1) was quantified. RM1-PSMA$^+$ cells were seeded at a density of 1×10^5 cells/well in 12-well plates, then incubated overnight. The cells were then treated with PBS, ^{161}Tb−S1R/PSMA-P, or ^{177}Lu−S1R/PSMA-P at indicated concentrations (0.01, 0.1, and 1.0 MBq/mL) for 48 h. The culture medium was then collected in order to ascertain the secretion of ATP and HMGB1 via an enhanced ATP assay kit and a mouse HMGB1 ELISA kit. The cells were collected and stained with an anti-CRT antibody at 4 °C for 1 h and Alexa Fluor 647-conjugated secondary antibody at 4 °C for 30 min, followed by flow cytometry analysis. The data were analyzed using FlowJo_V10.

In the subsequent stage of the study, the effects of radioligands-induced ICD on bone marrow-derived dendritic cells (BMDCs) were investigated. In this study, RM1-PSMA$^+$ cells were seeded in 12-well plates at a density of 1×10^5 cells/well. The cells were then incubated with radioligands at 0.1 MBq/mL (1 mL) for a period of 48 h. Following this, BMDCs (1×10^6/well) were added to each well and cocultured for a further 24 h. The culture medium was then collected in order to analyze the levels of cytokines, such as IL-6 and TNF-α, using ELISA kit specifically designed for mouse IL-6 and TNF-α, respectively. The cells were collected and stained with CD11c-FITC, CD80-APC, and CD86-PE/Cy7 antibodies, followed using flow cytometry. The data were analyzed using FlowJo_V10.

To compare the synergistic effects of ^{177}Lu−S1R/PSMA-P and ^{161}Tb−S1R/PSMA-P with immunotherapy, two parallel therapeutic experiments were conducted. In order to ascertain the effectiveness of the combination of ^{177}Lu−S1R/PSMA-P and αPD1, RM1-PSMA$^+$/RM1 tumor-bearing mice were methodically separated into six groups (n = 5) for the purpose of the study: PBS, ^{177}Lu−S1R/PSMA-P (3.7 MBq), ^{177}Lu−S1R/PSMA-P (7.4 MBq), αPD1 (10 μg/dose), ^{177}Lu−S1R/PSMA-P (3.7 MBq) + αPD1 (10 μg/dose), and ^{177}Lu−S1R/PSMA-P (7.4 MBq) + αPD1 (10 μg/dose). On day 0, ^{177}Lu−S1R/PSMA-P was administered intravenously, and αPD1 was given intravenously on days 1, 3, 5, and 7. The investigation into the efficacy of the combination of ^{161}Tb−S1R/PSMA-P and αPD1 involved the utilization of RM1-PSMA$^+$/RM1 tumor-bearing mice, which were randomly divided into four groups of six mice each: PBS, ^{161}Tb−S1R/PSMA-P (3.7 MBq), αPD1 (10 μg/dose), and ^{161}Tb−S1R/PSMA-P (3.7 MBq) + αPD1 (10 μg/dose). On day 0, ^{161}Tb−S1R/PSMA-P was administered intravenously, and αPD1 was given intravenously on days 1, 3, 5, and 7. Tumor volume and body weight were monitored on a twice-weekly basis, and the survival of the mouse was recorded. Mice were euthanized in accordance with established ethical protocols when they exhibited signs of distress or rapid weight loss (20% of

https://doi.org/10.1021/acs.molpharmaceut.6c00650
Mol. Pharmaceutics 2026, 23, 4311−4321

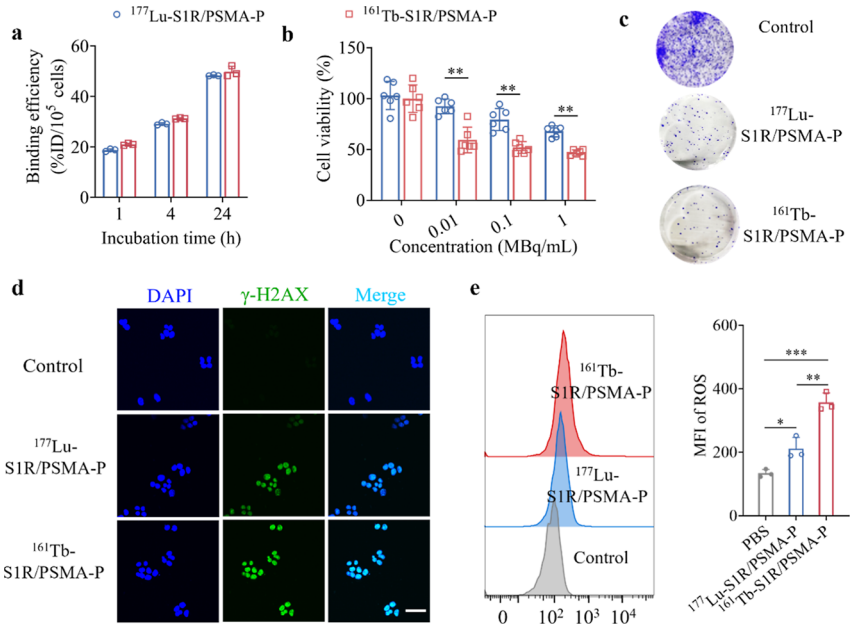

Figure 1. Binding and in vitro toxic effect of ^{161}Tb−S1R/PSMA-P compared with ^{177}Lu−S1R/PSMA-P in RM1-PSMA^{+} cells. (a) Cell binding efficiency after 1, 4, or 24 h incubation (n = 3). (b) Cytotoxicity of ^{177}Lu−S1R/PSMA-P and ^{161}Tb−S1R/PSMA-P in RM1-PSMA^{+} cells after 48 h incubation (n = 6). (c) Representative colony formation assay after 48 h incubation with radioligands (0.1 MBq/mL). (d) Representative confocal microscopy images of RM1-PSMA^{+} cells stained with γ-H2AX antibody after 48 h incubation with radioligands (0.1 MBq/mL) (scale bars: 50 μm). (e) Representative flow cytometry graph and mean fluorescence intensity (MFI) of ROS after 48 h incubation with radioligands (0.1 MBq/mL). Statistical significance was analyzed by one-way ANOVA, *p < 0.05, **p < 0.01, and ***p < 0.001.

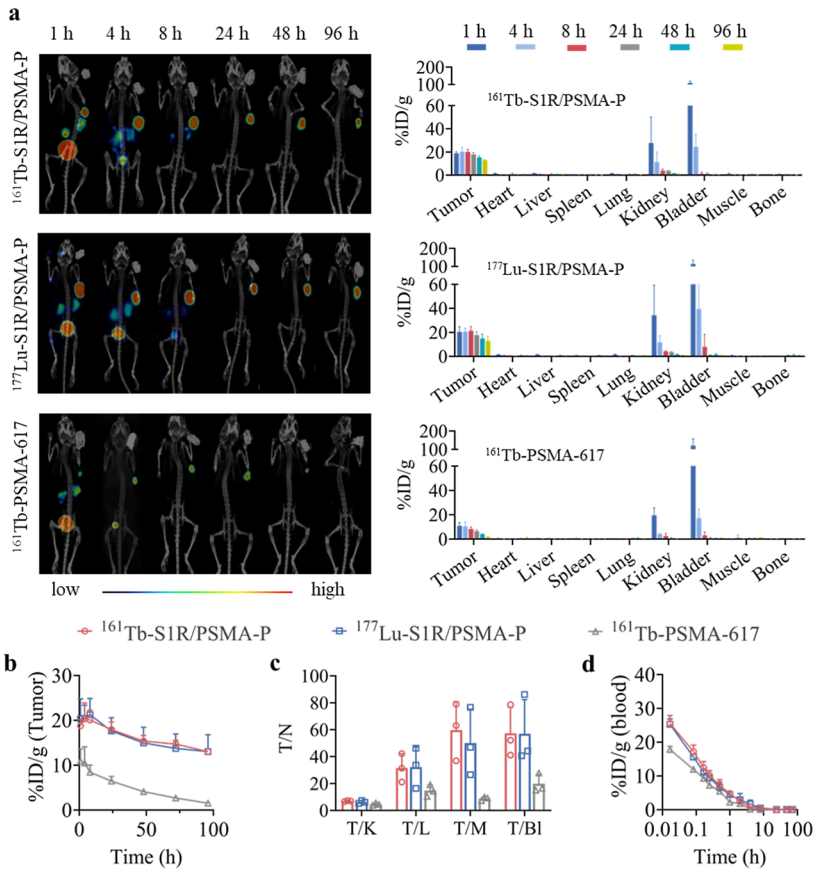

Figure 2. (a) SPECT/CT images of RM1-PSMA^{+}/RM1 tumor-bearing mice intravenously injected with ^{161}Tb−S1R/PSMA-P (11.1 MBq), ^{177}Lu−S1R/PSMA-P (11.1 MBq), and ^{161}Tb-PSMA-617 (11.1 MBq) (n = 3). (b) Accumulation of the radioligands in tumor. (c) Tumor-to-normal tissue (T/N) ratio. T: tumor, L: liver, M: muscle, B: bone. (d) The pharmacokinetics of radioligands in healthy male C57BL/6 mice after intravenous administration (5.5 MBq) (n = 3).

https://doi.org/10.1021/acs.molpharmaceut.6c00650
Mol. Pharmaceutics 2026, 23, 4311−4321

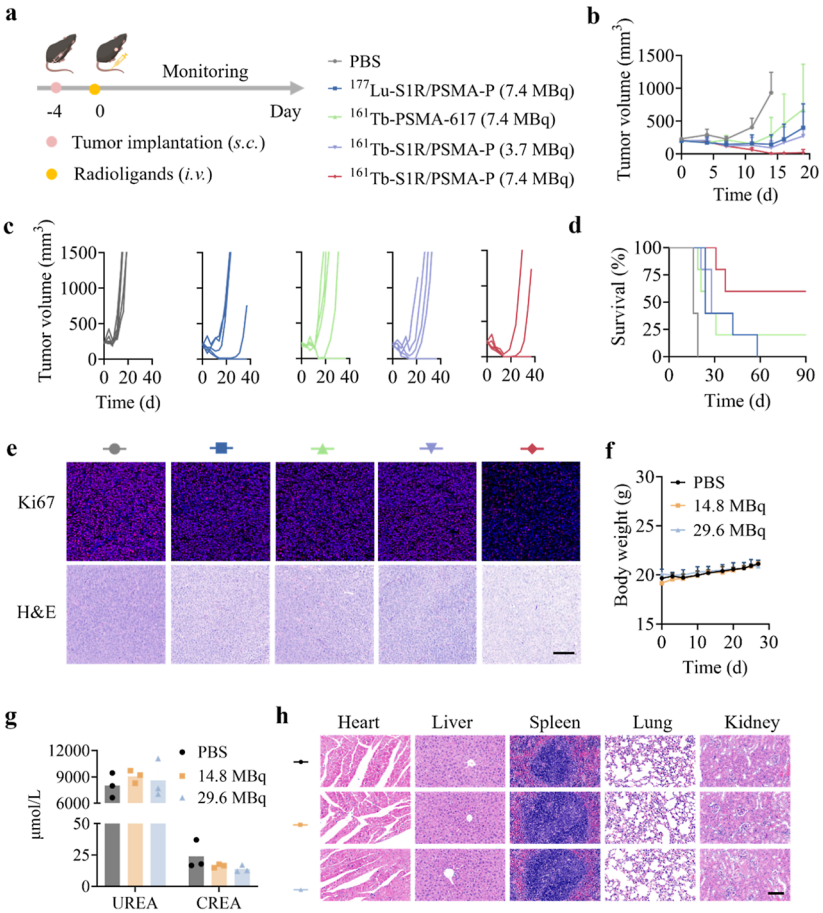

Figure 3. Therapeutic activity of ^{161}Tb−S1R/PSMA-P in RM1-PSMA^{+}/RM1 tumor-bearing mice (a−e) and safety evaluation of ^{161}Tb−S1R/PSMA-P in healthy C57BL/6 mice (f−h). (a) Experimental schedule for figures b, c, d, and e. (b) Average tumor growth curves, (c) individual tumor growth curves, and (d) Kaplan−Meier survival curves of the mice treated with ^{161}Tb−S1R/PSMA-P (3.7 or 7.4 MBq), ^{177}Lu−S1R/PSMA-P (7.4 MBq), and ^{161}Tb-PSMA-617 (7.4 MBq) (n = 5). (e) Representative immunofluorescence images of Ki67 and H&E-staining images of tumor slices on day 7 after intravenous injection of radioligands. Body weight changes (f), kidney function tests (g), and H&E staining of major organs (h) from healthy mice on day 27 post intravenous injection of ^{161}Tb−S1R/PSMA-P at doses of 14.8 and 29.6 MBq. Scale bar corresponds to 100 μm. UREA: urea, CREA: creatinine.

initial weight), tumor length exceeding 15 mm, or tumor volume surpassing 1500 mm^3.

In order to investigate the memory effect of combined radiotherapy and immunotherapy, three mice that had been cured were rechallenged with a mixture of RM1-PSMA^{+} cells (4.5×10^6 cells) and RM1 cells (5×10^5 cells) on day 90 after the initial ^{161}Tb−S1R/PSMA-P injection. Naïve mice that had been inoculated with the same cell mixture were used as a control group. Tumor volume and body weight were monitored twice a week, and survival was recorded. Following a rechallenge 11 days later, blood samples were collected and stained with CD3-APC, CD8-PE/Cy7, CD4-PE/Cy7, CD44-FITC, and CD62L-PE. The cells were analyzed via flow cytometry.

2.7. Immunological Analysis

In order to examine the immune responses to targeted radionuclide therapy combined with immunotherapy, RM1-PSMA^{+}/RM1 tumor-bearing mice were randomly divided into four groups (n = 4): PBS, TRT (^{161}Tb−S1R/PSMA-P: 3.7 MBq), αPD1 (10 μg), and TRT + αPD1 (^{161}Tb−S1R/PSMA-P: 3.7 MBq; αPD1: 10 μg). ^{161}Tb−S1R/PSMA-P was administered intravenously on day 0 and αPD1 was given intravenously on days 1, 3, and 5. On the seventh day, the tumors were harvested and dissociated into single-cell suspensions. Then cells were then stained with Zombie-NIR, blocked with antimouse CD16/32, and labeled with CD45.2-PerCP/Cy5.5, CD3-APC, CD8a-FITC, and CD4-PE in order to facilitate flow cytometry analysis. Serum samples were obtained in order to quantify the concentrations of IFN-γ and TNF-α. One mouse from each group was euthanized for the purpose of tumor excision, which was then subjected to staining with anti-CD4 and anti-CD8 primary antibodies, as well as Alexa Fluor 647 secondary antibody staining, for the purpose of observation under a confocal microscope.

3. RESULTS AND DISCUSSION

3.1. Radiosynthesis and In Vitro Antitumor Efficacy

S1R/PSMA-P was efficiently labeled with ^{161}Tb under the same conditions for ^{177}Lu. Radio-TLC analysis demonstrated that ^{161}Tb−S1R/PSMA-P attained a radiochemical yield that surpassed 99%, following a 15 min reaction at 95 °C (Figure S1). Furthermore, ^{161}Tb−S1R/PSMA-P displayed exceptional radiostability in PBS and 10% FBS at ambient temperature, preserving radiochemical purity above 95% for a duration of 7 days (Figure S2). This radiostability profile is comparable to that previously reported for ^{177}Lu−S1R/PSMA-P.[28] Moreover, ^{161}Tb−S1R/PSMA-P exhibits comparable binding affinity to RM1-PSMA^{+} cells to ^{177}Lu−S1R/PSMA-P (Figure 1a). This finding indicates that substituting ^{177}Lu with ^{161}Tb exerts a negligible influence on the cellular binding, which is in accordance with previous report.[33] ^{161}Tb−S1R/PSMA-P demonstrated 1.4- to 1.6-fold greater inhibitory potency in RM1-PSMA^{+} cells than ^{177}Lu−S1R/PSMA-P (Figure 1b). At a

https://doi.org/10.1021/acs.molpharmaceut.6c00650
Mol. Pharmaceutics 2026, 23, 4311−4321

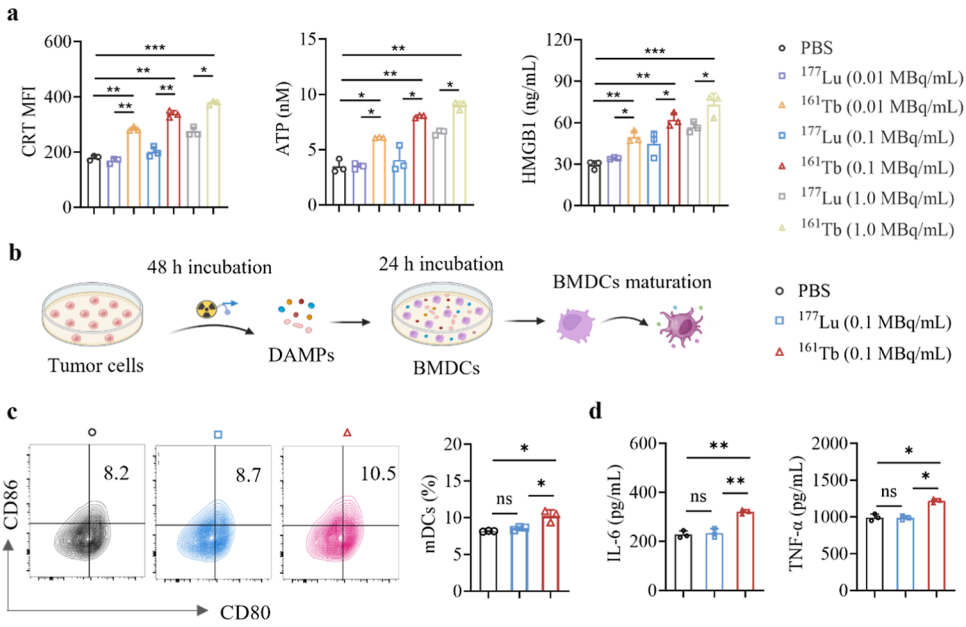

Figure 4. Comparative in vitro immunostimulatory capacity of ^{161}Tb−S1R/PSMA-P and ^{177}Lu−S1R/PSMA-P (n = 3). (a) MFI of surface CRT exposure, ATP release, and HMGB1 release in RM1-PSMA$^+$ cells treated with ^{161}Tb−S1R/PSMA-P or ^{177}Lu−S1R/PSMA-P at indicated concentrations (0.01, 0.1, and 1.0 MBq/mL) for 48 h. (b) Schematic illustration of the BMDCs activation for figures c-d. (c) Representative flow cytometry graphs and percentage of mature BMDCs (CD11c$^+$CD80$^+$CD86$^+$, mDCs). (d) Concentrations of IL-6 and TNF-α secreted in the supernatants of BMDCs. Statistical significance was analyzed by one-way ANOVA, *p < 0.05, **p < 0.01, and ***p < 0.001.

concentration of 0.1 MBq/mL, ^{161}Tb−S1R/PSMA-P reduced cell viability to 51.9% ± 5.3%. This enhanced efficacy of ^{161}Tb−S1R/PSMA-P was further confirmed by the colony-forming assay (Figure 1c). ^{161}Tb−S1R/PSMA-P showed a propensity to induce a greater number of DNA double-strand breaks and ROS (Figure 1d,e). At equivalent radioactivity levels, the ROS intensity of ^{161}Tb−S1R/PSMA-P was found to be 1.6× that of ^{177}Lu−S1R/PSMA-P. Furthermore, the computational results showed that the production of radicals was 1.5× higher for ^{161}Tb than for ^{177}Lu. The above findings provide direct experimental validation that the unique decay profile of ^{161}Tb, specifically its coemission of Auger electrons, translates into superior radiotoxic efficacy compared to ^{177}Lu.

3.2. Biodistribution Study

^{161}Tb emits γ rays suitable for SPECT imaging, enabling in vivo profiling of biodistribution.[34−36] The microSPECT/CT imaging in RM1-PSMA$^+$/RM1 tumor-bearing mice revealed that ^{161}Tb−S1R/PSMA-P had notable tumor uptake, reaching 20.3 ± 2.9%ID/g at 4 h postinjection and maintaining 13.0 ± 0.4%ID/g at 96 h postinjection (Figure 2a). Importantly, ^{161}Tb−S1R/PSMA-P exhibited rapid renal clearance and minimal distribution in the healthy organs, which was analogous to that of ^{177}Lu−S1R/PSMA-P. Over the observation period (1−96 h), ^{161}Tb−S1R/PSMA-P agents demonstrated 3.1-fold higher tumor accumulation and 1.2- to 6.7-fold higher tumor-to normal tissue (T/N) ratios compared to ^{161}Tb-PSMA-617 (Figure 2b,c). These elevated T/N ratios indicated superior selectivity and a more favorable therapeutic index for ^{161}Tb−S1R/PSMA-P. ^{161}Tb−S1R/PSMA-P was rapidly eliminated from the bloodstream with a half-life of 0.16 h (Figure 2d), which was consistent with the high hydrophilicity of S1R/PSMA-P (log P = −3.3 ± 0.03), despite being slightly less hydrophilic than PSMA-617 (reported log P = −4.0 ± 0.15).[37] These findings suggest that ^{161}Tb and ^{177}Lu-labeled S1R/PSMA-P have similar pharmacokinetics and biodistribution profiles. The consistently superior tumor uptake and enhanced tumor-to-normal tissue ratios demonstrated by ^{161}Tb−S1R/PSMA-P compared to ^{161}Tb-PSMA-617 validates the advantage of the dual-targeted strategy in improving the specificity and therapeutic index for prostate cancer.

3.3. Targeted Radionuclide Therapy

The in vivo antitumor efficacy of these radioligands was evaluated in RM1-PSMA$^+$/RM1 tumor-bearing mice (Figure 3a). Figure 3b shows that, at equivalent doses, the therapeutic efficacy of ^{161}Tb−S1R/PSMA-P is superior to that of both ^{177}Lu−S1R/PSMA-P and ^{161}Tb-PSMA-617. Notably, the antitumor efficacy of a single dose of ^{161}Tb−S1R/PSMA-P (3.7 MBq) is similar to that of ^{177}Lu−S1R/PSMA-P (7.4 MBq) and greater than that of ^{161}Tb-PSMA-617 (7.4 MBq). Previous studies have reported similar targeting but enhanced therapeutic efficacy for ^{161}Tb-labeled radioligands relative to their ^{177}Lu analogs.[38,39] Consistent with this, ^{161}Tb−S1R/PSMA-P and ^{177}Lu−S1R/PSMA-P showed comparable cellular uptake and tumor accumulation, suggesting similar receptor-mediated internalization. Moreover, S1R/PSMA-P has been shown to exhibit greater cellular internalization and retention than PSMA-617,[29] which may contribute to the superior efficacy of ^{161}Tb−S1R/PSMA-P over ^{161}Tb-PSMA-617. Remarkably, a single 7.4 MBq dose of ^{161}Tb−S1R/PSMA-P achieves a 60% tumor complete regression (CR), and even a 3.7 MBq dose yields a 20% CR (Figure 3c, d). Moreover, no significant body weight loss was observed during the treatments, indicating good tolerability (Figure S3). Consistent with the antitumor efficacy results, tumor slices from ^{161}Tb−S1R/PSMA-P (7.4 MBq) group displayed the lowest proliferation rate and the most extensive tumor necrosis compared to other groups (Figure 3e). These findings highlight the superior antitumor activity of ^{161}Tb−S1R/PSMA-P over ^{177}Lu−S1R/PSMA-P and ^{161}Tb-PSMA-617.

https://doi.org/10.1021/acs.molpharmaceut.6c00650
Mol. Pharmaceutics 2026, 23, 4311−4321

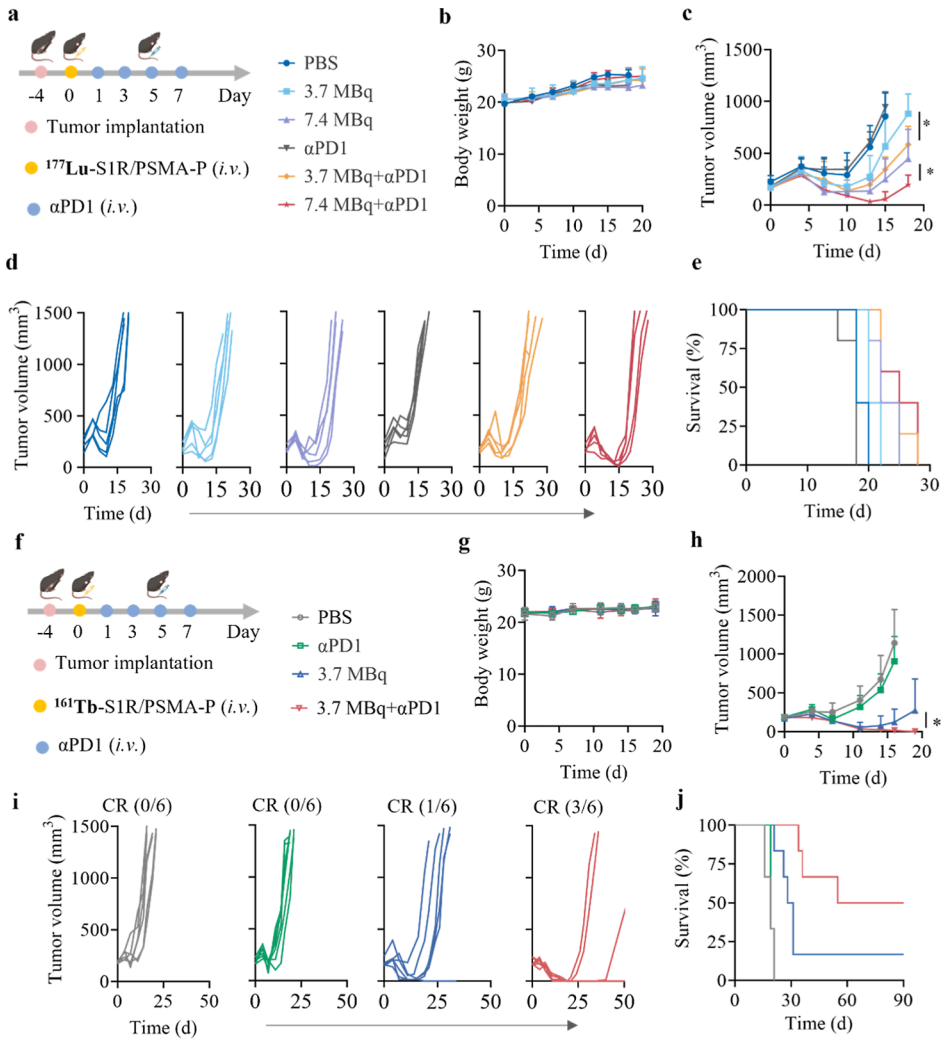

Figure 5. Sensitization effects of ^{177}Lu−S1R/PSMA-P to αPD1 therapy (a−e) and ^{161}Tb−S1R/PSMA-P to αPD1 therapy (f−j) in RM1-PSMA$^+$/RM1 tumor-bearing mice. (a) Experimental schedule for figures b-e (n = 5). (b) Average body weight of the mice. Average tumor growth curves (c), individual tumor growth (d) and survival curves (e). (f) Experimental schedule for figures g−j (n = 6). Average body weight (g), average tumor growth (h), individual tumor growth (i) and survival curves (j). Statistical significance was analyzed by one-way ANOVA and Log-rank test, *p < 0.05.

Furthermore, the safety of ^{161}Tb−S1R/PSMA-P was assessed in healthy mice. Figure 3f showed that a single injection of ^{161}Tb−S1R/PSMA-P at 14.8 and 29.6 MBq did not result in any loss of body weight over 27 days. Routine blood analysis revealed that white blood cell, red blood cell, and platelet levels were within normal ranges (Figure S4). Liver and kidney function tests of mice treated with ^{161}Tb−S1R/PSMA-P exhibited no significant differences compared to healthy mice (Figure 3g). Furthermore, no tissue abnormalities were observed in the main organs (Figure 3h). These results demonstrate that ^{161}Tb−S1R/PSMA-P is well tolerated. Notably, a half dose (3.7 MBq) of ^{161}Tb−S1R/PSMA-P was found to be as effective as a full dose (7.4 MBq) of the ^{177}Lu-labeled ligand, highlighting a significant therapeutic advantage.

3.4. ^{161}Tb−S1R/PSMA-P Boosts ICB Therapy

It has been reported that TRT can induce ICD by releasing DAMPs, which are characterized by the exposure of CRT and the release of ATP and HMGB1.[40,41] As illustrated in Figure 4a, RM1-PSMA$^+$ cells treated with ^{161}Tb−S1R/PSMA-P (0.01, 0.1, and 1.0 MBq/mL) for 48 h exhibited significant upregulation of CRT expression, as well as a marked increase in the release of ATP and HMGB1. In addition, ^{161}Tb−S1R/PSMA-P produced a remarkable release of DAMPs compared to ^{177}Lu−S1R/PSMA-P at the same dose. These results suggest that ^{161}Tb−S1R/PSMA-P can induce stronger ICD than ^{177}Lu−S1R/PSMA-P. The DAMPs released during ICD can be captured by antigen-presenting cells, such as DCs, promoting their maturation and antigen presentation to T cells, thereby activating the immune response.[42,43] To determine the degree of DCs stimulated by ICD effect, BMDCs were cocultured with RM1-PSMA$^+$ cells treated with radioligands for 24 h and analyzed by flow cytometry (Figure 4b). Treatment of RM1-PSMA$^+$ cells with ^{161}Tb−S1R/PSMA-P at 0.1 MBq/mL increased the proportion of mature BMDCs (CD11c$^+$CD80$^+$CD86$^+$, mDCs) from 8.2 ± 0.1% to 10.3 ± 0.8% (Figure 4c). In the supernatant of BMDCs, ^{161}Tb−S1R/PSMA-P group at 0.1 MBq/mL revealed 1.4- and 1.2-fold higher levels of IL-6 and TNF-α compared to the PBS group, respectively (Figure 4d). In contrast, treatment with ^{177}Lu−S1R/PSMA-P (0.1 MBq/mL) failed to induce significant BMDCs maturation compared to the PBS group. Therefore, ^{161}Tb−S1R/PSMA-P stimulated a higher proportion of

https://doi.org/10.1021/acs.molpharmaceut.6c00650
Mol. Pharmaceutics 2026, 23, 4311−4321

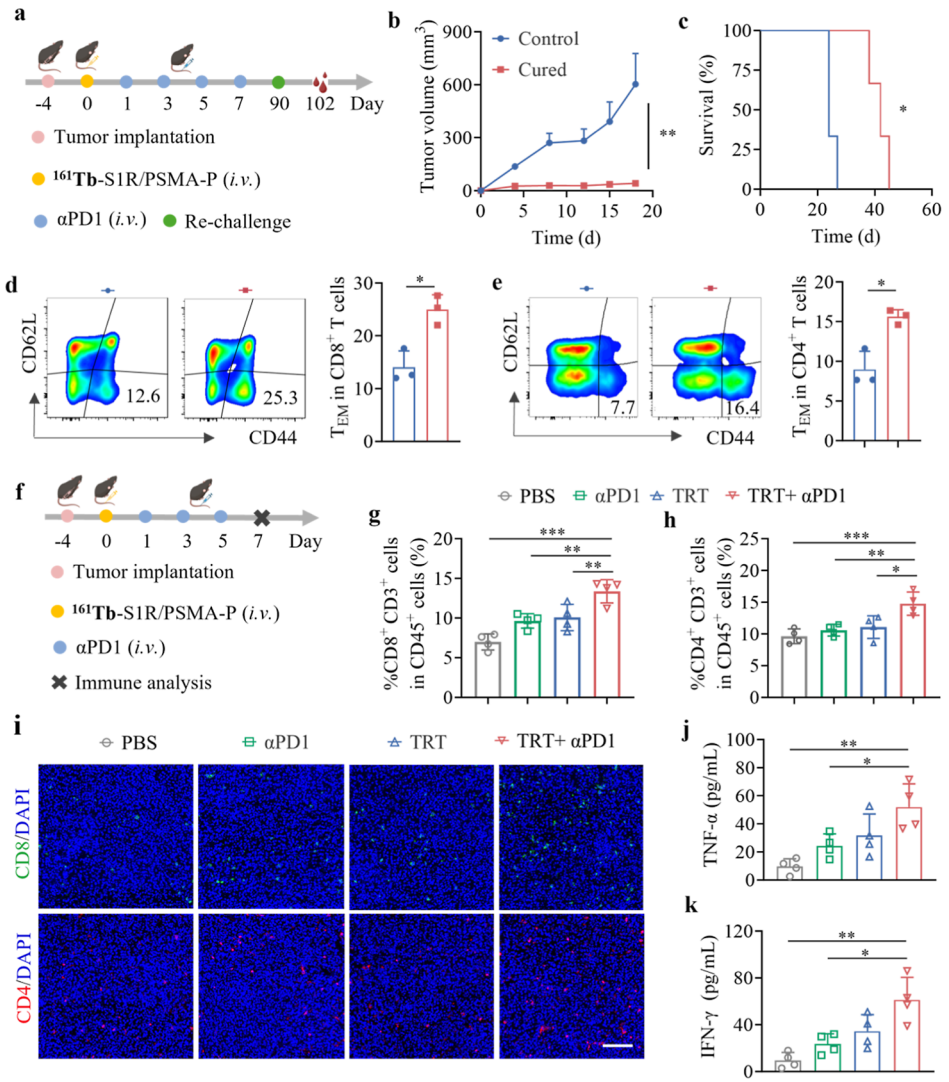

Figure 6. Antitumor memory (a–e) and immune regulation (f–k) of ^{161}Tb–S1R/PSMA-P combined with αPD1 in RM1-PSMA$^+$/RM1 tumor-bearing mice. (a) Experimental schedule for figures b–d (n = 3). Tumor growth (b) and survival curves (c) of mice rechallenged at day 90 after ^{161}Tb–S1R/PSMA-P treatment. Representative flow cytometry graphs and percentages of effector memory T cells in CD8$^+$ T (d) and in CD4$^+$ T (e) in peripheral blood following rechallenge. (f) Experimental workflow of immunotherapy and analysis of immune responses for g–k (n = 4). CD3$^+$CD8$^+$ T cells in CD45$^+$ cells (g) and CD3$^+$CD4$^+$ T cells in CD45$^+$ cells (h) within tumors. (i) Representative fluorescence microscopy images of CD8$^+$ T cells and CD4$^+$ T cells staining tumor slices. Scale bar: 100 μm. Serum concentrations of TNF-α (j) and IFN-γ (k) measured by ELISA. Statistical significance was analyzed by one-way ANOVA, *p < 0.05, **p < 0.01, and ***p < 0.001.

BMDCs maturation and secretion of immunostimulatory factors than ^{177}Lu–S1R/PSMA-P. Besides ICD-mediated DCs activation, the cGAS-STING pathway may also contribute to the enhanced immunostimulatory effects of ^{161}Tb–S1R/PSMA-P. Currenti et al. reported that ^{161}Tb induced more extensive DNA damage responses than ^{177}Lu,[44] which may facilitate cytosolic DNA accumulation and subsequent cGAS-STING activation,[45] potentially contributing to the enhanced immune activation induced by ^{161}Tb–S1R/PSMA-P. These mechanisms may collectively contribute to the superior ability of ^{161}Tb–S1R/PSMA-P to sensitize ICB therapy.

Next, the therapeutic effects of ^{161}Tb–S1R/PSMA-P and ^{177}Lu–S1R/PSMA-P in combination with immune checkpoint inhibitors were investigated. Two doses of ^{177}Lu–S1R/PSMA-P combined with αPD1 were selected (Figure 5a). The combination therapy did not induce any body weight loss (Figure 5b) and effectively controlled tumor volume during the initial stage (days 0 to 18) (Figure 5c). However, tumors subsequently entered a phase of accelerated proliferation (Figure 5d). Ultimately, ^{177}Lu-based combination failed to significantly extend overall survival (Figure 5e). These findings align with a previous study, which reported a similarly limited therapeutic outcome when combining ^{177}Lu-D3–6 and αPD1 in the 4T1 tumor model.[46] Subsequently, the therapeutic effects of ^{161}Tb–S1R/PSMA-P in combination with αPD1 were explored in RM1-PSMA$^+$/RM1 tumor-bearing mice (Figure 5f). Given that ^{161}Tb–S1R/PSMA-P at 7.4 MBq has been shown to achieve a 60% tumor-free rate, 3.7 MBq was selected for the purpose of evaluating the potential of ^{161}Tb–S1R/PSMA-P to sensitize αPD1. In a manner analogous to the combination of ^{177}Lu–S1R/PSMA-P with αPD1, the combination of ^{161}Tb–S1R/PSMA-P and αPD1 demonstrated no occurrence of body weight loss (Figure 5g). However, the combination of ^{161}Tb–S1R/PSMA-P and αPD1 demonstrated significantly enhanced tumor suppression (Figure 5h). It is

https://doi.org/10.1021/acs.molpharmaceut.6c00650
Mol. Pharmaceutics 2026, 23, 4311–4321

noteworthy that this combination successfully achieved a 50% tumor-free rate within a 90 day observation period, and significantly extended survival (Figure 5i,j). In summary, in contrast to ^{177}Lu−S1R/PSMA-P, ^{161}Tb−S1R/PSMA-P can effectively sensitize "cold" prostate cancer to αPD1 therapy.

In order to further evaluate the immune memory generated by the combination therapy, the cured mice were rechallenged with a mixture of RM1-PSMA$^+$ and RM1 on day 90 after the initial TRT. As illustrated in Figure 6a, the growth of tumors in the cured mice was effectively inhibited, and their survival was significantly prolonged in comparison to that of the naïve control group (24 d vs 42 d), suggesting ^{161}Tb−S1R/PSMA-P in combination with αPD1 induced enhanced and protective immune memory (Figure 6b, c). Eleven days postrechallenge, the effector memory T cells were analyzed in the peripheral blood. CD8$^+$ effector memory T cells and CD4$^+$ effector memory T cells are critical for mediating rapid recall responses upon antigen re-exposure.[47,48] Flow cytometric analysis revealed that the frequencies of both CD8$^+$ effector memory T cells (CD8$^+$CD44$^+$CD62L$^-$) and CD4$^+$ effector memory T cells (CD4$^+$CD44$^+$CD62L$^-$) increased from 14.1 ± 3.1% to 25.0 ± 2.8% and 9.0 ± 2.3% to 15.9 ± 1.2%, respectively (Figure 6d,e), indicating a robust immune memory response against tumor recurrence.

Subsequent investigation was directed toward the immunological responses of mice following combination therapy (Figure 6f). ^{161}Tb−S1R/PSMA-P (3.7 MBq) was administered intravenously, and αPD1 (10 μg/dose) was given intravenously on days 1, 3, and 5. The immune response analysis of tumor was conducted on day 7. The results demonstrated that the combination of ^{161}Tb−S1R/PSMA-P and αPD1 led to a substantial augmentation in the proportion of CD8$^+$ T cells (CD45$^+$CD3$^+$CD8$^+$) and CD4$^+$ T cells (CD45$^+$CD3$^+$CD4$^+$) within the tumor (Figure 6g,h), a phenomenon that was corroborated by the fluorescence microscopy images of tumor slices (Figure 6i). Combo therapy also led to an increase in serum TNF-α and IFN-γ secretion (Figure 6j,k), indicating that this strategy not only elicits a local antitumor immune response but also triggers a systemic antitumor immune response.

Furthermore, the safety of combo therapy was investigated in healthy mice. Throughout the whole observation period, no body weight loss was observed (Figure S5a). The combo therapy exhibited minimal impact on blood routine analysis and liver and kidney function tests (Figure S5b,c). Histological analysis revealed that no detectable damage to major organs was caused by combo therapy (Figure S5d). These results highlight the excellent efficacy and safety of ^{161}Tb−S1R/PSMA-P and αPD1 combo therapy.

4. CONCLUSION

We have demonstrated that extracellular-intracellular dual-targeted radionuclide therapy with ^{161}Tb effectively inhibits murine prostate tumor and instigates potent anticancer immunity. In comparison with its ^{177}Lu counterpart, ^{161}Tb−S1R/PSMA-P induces besides enhanced radiotoxicity significantly more ICD and DCs maturation. Interestingly, a single dose of ^{161}Tb−S1R/PSMA-P at 7.4 MBq cures 60% of RM1-PSMA$^+$/RM1 tumor-bearing mice, greatly outperforming ^{177}Lu−S1R/PSMA-P as well as ^{161}Tb-PSMA-617. We further showed that ^{161}Tb−S1R/PSMA-P at a dose of 3.7 MBq effectively sensitizes RM1-PSMA$^+$/RM1 tumor to αPD1 immune checkpoint blockade therapy, which affords powerful and durable antitumor immunity. ^{161}Tb−S1R/PSMA-P with favorable features like high tumor selectivity, uptake and retention, and elevated tumor radiotoxicity and immune activation has emerged as a next-generation radiopharmaceutics for advanced prostate cancer.

■ ASSOCIATED CONTENT

Data Availability Statement

Data is available upon request.

Supporting Information

The Supporting Information is available free of charge at https://pubs.acs.org/doi/10.1021/acs.molpharmaceut.6c00650.

Supplementary Figures (S1−S2): radiolabeling efficiency of ^{161}Tb−S1R/PSMA-P and ^{177}Lu−S1R/PSMA-P; radiostability of ^{161}Tb−S1R/PSMA-P in PBS or 10% FBS. Supplementary Figures (S3−S5): body weight changes of mice treated with ^{161}Tb−S1R/PSMA-P, ^{177}Lu−S1R/PSMA-P, or ^{161}Tb-PSMA-617; routine blood analysis following ^{161}Tb−S1R/PSMA-P administration, and safety assessment of ^{161}Tb−S1R/PSMA-P combined with αPD1, including body weight, hematological parameters, liver and kidney function, and H&E staining of major organs (PDF)

■ AUTHOR INFORMATION

Corresponding Authors

Guanglin Wang − *State Key Laboratory of Radiation Medicine and Protection, School of Radiation Medicine and Protection, Collaborative Innovation Center of Radiation Medicine of Jiangsu Higher Education Institutions, Soochow University, Suzhou 215123, China;* orcid.org/0000-0002-6463-119X; Email: glwang@suda.edu.cn

Zhiyuan Zhong − *State Key Laboratory of Radiation Medicine and Protection, School of Radiation Medicine and Protection, Collaborative Innovation Center of Radiation Medicine of Jiangsu Higher Education Institutions, Soochow University, Suzhou 215123, China;* orcid.org/0000-0003-4175-4741; Email: zyzhong@suda.edu.cn

Authors

Juan Sun − *College of Pharmaceutical Sciences, Soochow University, Suzhou 215123, China*

Jiakun Guo − *College of Pharmaceutical Sciences, Soochow University, Suzhou 215123, China*

Xunhao Qi − *State Key Laboratory of Radiation Medicine and Protection, School of Radiation Medicine and Protection, Collaborative Innovation Center of Radiation Medicine of Jiangsu Higher Education Institutions, Soochow University, Suzhou 215123, China*

Jiangtao Yang − *College of Pharmaceutical Sciences, Soochow University, Suzhou 215123, China*

Guangming Zhou − *State Key Laboratory of Radiation Medicine and Protection, School of Radiation Medicine and Protection, Collaborative Innovation Center of Radiation Medicine of Jiangsu Higher Education Institutions, Soochow University, Suzhou 215123, China;* orcid.org/0000-0001-5695-2308

Fenghua Meng − *College of Pharmaceutical Sciences, Soochow University, Suzhou 215123, China;* orcid.org/0000-0002-8608-7738

https://doi.org/10.1021/acs.molpharmaceut.6c00650
Mol. Pharmaceutics 2026, 23, 4311−4321

Complete contact information is available at:
https://pubs.acs.org/10.1021/acs.molpharmaceut.6c00650

Author Contributions

[§]J.S., J.G. and X.Q. contributed equally to this work. **Juan Sun**: Writing—original draft, Investigation, Formal analysis, Data curation, Conceptualization. **Jiakun Guo**: Validation, Project administration, Investigation, Formal analysis, Data curation. **Xunhao Qi**: Writing—original draft, Methodology, Investigation, Formal analysis, Data curation. **Jiangtao Yang**: Methodology, Investigation, Formal analysis, Data curation. **Guanglin Wang**: Writing—review and editing, Validation, Supervision, Resources, Data curation, Conceptualization. **Guangming Zhou**: Supervision, Resources, Project administration. **Fenghua Meng**: Supervision, Resources, Project administration, Investigation. **Zhiyuan Zhong**: Writing review and editing, Writing—original draft, Supervision, Funding acquisition, Conceptualization.

Funding

This work is supported by research grants from the National Natural Science Foundation of China (52233007).

Notes

Written Informed consent was obtained from all individual participants included in the study. The authors consent to publish.
The authors declare no competing financial interest.

REFERENCES

(1) Senior, M. Precision radiation opens a new window on cancer therapy. *Nat. Biotechnol.* **2024**, *42* (7), 1003−1008.
(2) Bodei, L.; Herrmann, K.; Schöder, H.; Scott, A. M.; Lewis, J. S. Radiotheranostics in oncology: current challenges and emerging opportunities. *Nat. Rev. Clin. Oncol.* **2022**, *19* (8), 534−550.
(3) Aboagye, E. O.; Barwick, T. D.; Haberkorn, U. Radiotheranostics in oncology: making precision medicine possible. *Ca-Cancer J. Clin.* **2023**, *73* (3), 255−274.
(4) Sun, J.; Huangfu, Z.; Yang, J.; Wang, G.; Hu, K.; Gao, M.; Zhong, Z. Imaging-guided targeted radionuclide tumor therapy: from concept to clinical translation. *Adv. Drug Delivery Rev.* **2022**, *190*, 114538.
(5) Jaffray, D. A.; Knaul, F.; Baumann, M.; Gospodarowicz, M. Harnessing progress in radiotherapy for global cancer control. *Nat. Cancer* **2023**, *4* (9), 1228−1238.
(6) Albert, N. L.; Le Rhun, E.; Minniti, G.; Mair, M. J.; Galldiks, N.; Tolboom, N.; Jakola, A. S.; Niyazi, M.; Smits, M.; Verger, A.; Cicone, F.; Weller, M.; Preusser, M. Translating the theranostic concept to neuro-oncology: Disrupting barriers. *Lancet Oncol.* **2024**, *25* (9), 441−451.
(7) Pomykala, K. L.; Hadaschik, B. A.; Sartor, O.; Gillessen, S.; Sweeney, C. J.; Maughan, T.; Hofman, M. S.; Herrmann, K. Next generation radiotheranostics promoting precision medicine. *Ann. Oncol.* **2023**, *34* (6), 507−519.
(8) Sonbol, M. B.; Halfdanarson, T. R.; Hilal, T. Assessment of therapy-related myeloid neoplasms in patients with neuroendocrine tumors after peptide receptor radionuclide therapy: a systematic review. *JAMA Oncol* **2020**, *6* (7), 1086−1092.
(9) Parihar, A. S.; Hofman, M. S.; Iravani, A. 177Lu-Prostate-specific membrane antigen radioligand therapy in patients with metastatic castration-resistant prostate cancer. *Radiology* **2023**, *306* (2), 220859−220867.
(10) Strosberg, J.; El-Haddad, G.; Wolin, E.; Hendifar, A.; Yao, J.; Chasen, B.; Mittra, E.; Kunz, P. L.; Kulke, M. H.; Jacene, H.; Bushnell, D.; O'Dorisio, T. M.; Baum, R. P.; Kulkarni, H. R.; Caplin, M.; Lebtahi, R.; Hobday, T.; Delpassand, E.; Van Cutsem, E.; Benson, A.; Srirajaskanthan, R.; Pavel, M.; Mora, J.; Berlin, J.; Grande, E.; Reed, N.; Seregni, E.; Oberg, K.; Lopera Sierra, M.; Santoro, P.; Thevenet, T.; Erion, J. L.; Ruszniewski, P.; Kwekkeboom, D.; Krenning, E.; Investigators, N.-T. Phase 3 trial of 177Lu-Dotatate for midgut neuroendocrine tumors. *N. Engl. J. Med.* **2017**, *376* (2), 125−135.
(11) Feuerecker, B.; Tauber, R.; Knorr, K.; Heck, M.; Beheshti, A.; Seidl, C.; Bruchertseifer, F.; Pickhard, A.; Gafita, A.; Kratochwil, C.; Retz, M.; Gschwend, J. E.; Weber, W. A.; D'Alessandria, C.; Morgenstern, A.; Eiber, M. Activity and adverse events of actinium-225-PSMA-617 in advanced metastatic castration-resistant prostate cancer after failure of lutetium-177-PSMA. *Eur. Urol.* **2021**, *79* (3), 343−350.
(12) De Vincentis, G.; Gerritsen, W.; Gschwend, J. E.; Hacker, M.; Lewington, V.; O'Sullivan, J. M.; Oya, M.; Pacilio, M.; Parker, C.; Shore, N.; Sartor, O. Advances in targeted alpha therapy for prostate cancer. *Ann. Oncol.* **2019**, *30* (11), 1728−1739.
(13) Sathekge, M.; Morgenstern, A. Advances in targeted alpha therapy of cancer. *Eur. J. Nucl. Med. Mol. Imaging* **2024**, *51* (5), 1205−1206.
(14) McDevitt, M. R.; Ma, D.; Lai, L. T.; Simon, J.; Borchardt, P.; Frank, R. K.; Wu, K.; Pellegrini, V.; Curcio, M. J.; Miederer, M.; Bander, N. H.; Scheinberg, D. A. Tumor therapy with targeted atomic nanogenerators. *Science* **2001**, *294* (5546), 1537−1540.
(15) Ding, J.; Qin, S. S.; Hou, X. G.; Zhang, J. J.; Yang, M. D.; Ma, S. H.; Zhu, H.; Feng, Y. T.; Yu, F. Recent advances in emerging radiopharmaceuticals and the challenges in radiochemistry and analytical chemistry. *TrAC, Trends Anal. Chem.* **2025**, *182*, 118053−118073.
(16) Kong, G.; Buteau, J. P.; Hofman, M. S. Is 161Tb really happening? *J. Nucl. Med.* **2024**, *65* (5), 686−687.
(17) Borgna, F.; Haller, S.; Rodriguez, J. M. M.; Ginj, M.; Grundler, P.; Zeevaart, J. R.; Köster, U.; Schibli, R.; van der Meulen, N. P.; Müller, C. Combination of terbium-161 with somatostatin receptor antagonists-a potential paradigm shift for the treatment of neuroendocrine neoplasms. *Eur. J. Nucl. Med. Mol. Imaging* **2022**, *49* (4), 1113−1126.
(18) Verburg, F. A.; de Blois, E.; Koolen, S.; Konijnenberg, M. W. Replacing Lu-177 with Tb-161 in DOTA-TATE and PSMA-617 therapy: potential dosimetric implications for activity selection. *EJNMMI Phys.* **2023**, *10* (1), 69.
(19) Alcocer-Avila, M. E.; Ferreira, A.; Quinto, M. A.; Morgat, C.; Hindié, E.; Champion, C. Radiation doses from 161Tb and 177Lu in single tumour cells and micrometastases. *EJNMMI Phys.* **2020**, *7* (1), 33.
(20) Chen, L.; Xu, Y.-X.; Wang, Y.-S.; Ren, Y.-Y.; Dong, X.-M.; Wu, P.; Xie, T.; Zhang, Q.; Zhou, J.-L. Prostate cancer microenvironment: multidimensional regulation of immune cells, vascular system, stromal cells, and microbiota. *Mol. Cancer* **2024**, *23* (1), 229−260.
(21) Lyu, A.; Fan, Z. H.; Clark, M.; Lea, A.; Luong, D.; Setayesh, A.; Starzinski, A.; Wolters, R.; Arias-Badia, M.; Allaire, K.; Wu, K.; Gurunathan, V.; Valderrábano, L.; Wei, X. X.; Miller, R. A.; Van Allen, E. M.; Fong, L. Evolution of myeloid-mediated immunotherapy resistance in prostate cancer. *Nature* **2025**, *637* (8048), 1207−1217.
(22) Ghiringhelli, F.; Rébé, C. Using immunogenic cell death to improve anticancer efficacy of immune checkpoint inhibitors: From basic science to clinical application. *Immunol. Rev.* **2024**, *321* (1), 335−349.
(23) Shi, F.; Huang, X.; Hong, Z.; Lu, N.; Huang, X.; Liu, L.; Liang, T.; Bai, X. Improvement strategy for immune checkpoint blockade: a focus on the combination with immunogenic cell death inducers. *Cancer Lett.* **2023**, *562*, 216167.
(24) Kerr, C. P.; Jin, W. J.; Liu, P.; Grudzinski, J. J.; Ferreira, C. A.; Comas Rojas, H.; Oñate, A. J.; Kwon, O.; Hyun, M.; Bio Idrissou, M.; Welch Schwartz, R.; Vera, J. M.; Clark, P. A.; Adeniyi, A.; Takashima, M.; Erbe, A. K.; Shea, A. G.; Powers, M.; Pinchuk, A. N.; Massey, C. F.; Choi, C.; Hernandez, R.; Bednarz, B. P.; Ong, I. M.; Weichert, J. P.; Morris, Z. S. Priming versus propagating: distinct immune effects of alpha- versus beta-particle emitting radiopharmaceuticals when combined with immune checkpoint inhibition in mice. *Nat. Commun.* **2026**, *17* (1), 2044.

(25) Cui, X.-Y.; Li, Z.; Kong, Z.; Liu, Y.; Meng, H.; Wen, Z.; Wang, C.; Chen, J.; Xu, M.; Li, Y.; Gao, J.; Zhu, W.; Hao, Z.; Huo, L.; Liu, S.; Yang, Z.; Liu, Z. Covalent targeted radioligands potentiate radionuclide therapy. *Nature* **2024**, *630* (8015), 206−213.
(26) Galbiati, A.; Bocci, M.; Gervasoni, S.; Prodi, E.; Malloci, G.; Neri, D.; Cazzamalli, S. Molecular evolution of multivalent OncoFAP derivatives with enhanced tumor uptake and prolonged tumor retention. *J. Med. Chem.* **2024**, *67* (15), 13392−13408.
(27) Hu, B.; Liu, T.; Li, L.; Shi, L.; Yao, M.; Li, C.; Ma, X.; Zhu, H.; Jia, B.; Wang, F. IgG-binding nanobody capable of prolonging nanobody-based radiotracer plasma half-life and enhancing the efficacy of tumor-targeted radionuclide therapy. *Bioconjugate Chem.* **2022**, *33* (7), 1328−1339.
(28) Huangfu, Z.; Yang, J.; Sun, J.; Xu, B.; Tao, L.; Wu, J.; Wang, F.; Wang, G.; Meng, F.; Zhong, Z. PSMA and Sigma-1 receptor dual-targeted peptide mediates superior radionuclide imaging and therapy of prostate cancer. *J. Controlled Release* **2024**, *375*, 767−775.
(29) Sun, J.; Yang, J.; Guo, J.; Tao, L.; Xu, B.; Wang, G.; Meng, F.; Zhong, Z. Dual-targeted alpha therapy mitigates prostate cancer and boosts immune checkpoint blockade therapy. *J. Controlled Release* **2025**, *382*, 113686.
(30) Sun, J.; Yang, J.; Guo, J.; Xu, B.; Tao, L.; Zhao, X.; Wang, G.; Meng, F.; Zhong, Z. Naphthalene-containing octreotide radioligand elevates selectivity and radionuclide therapy for somatostatin receptor 2-positive tumor. *Colloid Surf. B-Biointerfaces* **2025**, *255*, 114945.
(31) Fendler, W. P.; Stuparu, A. D.; Evans-Axelsson, S.; Lückerath, K.; Wei, L.; Kim, W.; Poddar, S.; Said, J.; Radu, C. G.; Eiber, M.; Czernin, J.; Slavik, R.; Herrmann, K. Establishing (177)Lu-PSMA-617 radioligand therapy in a syngeneic model of murine prostate cancer. *J. Nucl. Med.* **2017**, *58* (11), 1786−1792.
(32) Guo, J.; Tan, H.; Chen, W.; Wang, Y.; Lin, W.; Zhong, Z.; Deng, C. Oncolytic microgels with regulated antibody release augment tumor immunotherapy. *J. Controlled Release* **2025**, *385*, 114003.
(33) Tschan, V. J.; Busslinger, S. D.; Bernhardt, P.; Grundler, P. V.; Zeevaart, J. R.; Köster, U.; van der Meulen, N. P.; Schibli, R.; Müller, C. Albumin-binding and conventional PSMA ligands in combination with (161)Tb: biodistribution, dosimetry, and preclinical therapy. *J. Nucl. Med.* **2023**, *64* (10), 1625−1631.
(34) Schaefer-Schuler, A.; Burgard, C.; Blickle, A.; Maus, S.; Petrescu, C.; Petto, S.; Bartholomä, M.; Stemler, T.; Ezziddin, S.; Rosar, F. [(161)Tb]Tb-PSMA-617 radioligand therapy in patients with mCRPC: preliminary dosimetry results and intra-individual head-to-head comparison to [(177)Lu]Lu-PSMA-617. *Theranostics* **2024**, *14* (5), 1829−1840.
(35) Al-Ibraheem, A.; Doudeen, R. M.; Juaidi, D.; Abufara, A.; Maus, S. Tb-PSMA radioligand therapy: first-in-humans SPECT/CT imaging. *J. Nucl. Med.* **2023**, *64* (8), 1322−1323.
(36) Baum, R. P.; Singh, A.; Kulkarni, H. R.; Bernhardt, P.; Rydén, T.; Schuchardt, C.; Gracheva, N.; Grundler, P. V.; Köster, U.; Müller, D.; Pröhl, M.; Zeevaart, J. R.; Schibli, R.; van der Meulen, N. P.; Müller, C. First-in-humans application of (161)Tb: a feasibility study using (161)Tb-DOTATOC. *J. Nucl. Med.* **2021**, *62* (10), 1391−1397.
(37) Benešová, M.; Umbricht, C. A.; Schibli, R.; Müller, C. Albumin-binding PSMA ligands: optimization of the tissue distribution profile. *Mol. Pharmaceutics* **2018**, *15* (3), 934−946.
(38) Holzleitner, N.; Cwojdzinski, T.; Beck, R.; Urtz-Urban, N.; Hillhouse, C. C.; Grundler, P. V.; van der Meulen, N. P.; Talip, Z.; Ramaekers, S.; Van de Voorde, M.; Ponsard, B.; Casini, A.; Günther, T. Preclinical evaluation of gastrin-releasing peptide receptor antagonists labeled with 161Tb and 177Lu: a comparative study. *J. Nucl. Med.* **2024**, *65* (3), 481−484.
(39) Kucuk, N. O.; Coskun, N.; Araz, M.; Alan Selcuk, N.; Berberoglu, K.; Ozdemir, E. C.; Gumuser, F. G.; Kuyumcu, S.; Sezgin, C.; Sanli, O.; Sanli, Y.; Sendur, M. A. N.; Urun, Y. Initial multicenter experience with 161Tb-PSMA in 177Lu-PSMA−refractory metastatic castration-resistant prostate cancer: preliminary results. *J. Nucl. Med.* **2025**, *66* (12), 1921−1926.
(40) Lunj, S.; Smith, T. A. D.; Reeves, K. J.; Currell, F.; Honeychurch, J.; Hoskin, P.; Choudhury, A. Immune effects of α and β radionuclides in metastatic prostate cancer. *Nat. Rev. Urol.* **2024**, *21* (11), 651−661.
(41) Kleinendorst, S. C.; Hooijmans, C. R.; Muselaers, S.; Oosterwijk, E.; Konijnenberg, M.; Heskamp, S.; van Lith, S. A. M. Efficacy of combined targeted radionuclide therapy and immune checkpoint Inhibition in animal tumour models: a systematic review and meta-analysis of the literature. *Eur. J. Nucl. Med. Mol. Imaging* **2025**, *52*, 4735−4751.
(42) He, Y.; Wu, S.; Yuan, Y.; Sun, Y.; Ai, Q.; Zhou, R.; Chai, G.; Chen, D.; Hu, H. Remodeling tumor immunosuppression with molecularly imprinted nanoparticles to enhance immunogenic cell death for cancer immunotherapy. *J. Controlled Release* **2023**, *362*, 44−57.
(43) Xiao, H.; Li, X.; Liang, S.; Yang, S.; Han, S.; Huang, J.; Shuai, X.; Ren, J. Dual-responsive nanomedicine activates programmed antitumor immunity through targeting lymphatic system. *ACS Nano* **2024**, *18* (17), 11070−11083.
(44) Rioja-Blanco, E.; Banz, Y.; Schlapbach, C.; Novak, U.; Chiorazzo, T.; Bertschi, N. L.; Bernhardt, P.; Grundler, P. V.; van der Meulen, N. P.; Grzmil, M.; Schibli, R.; Behe, M. 161Tb radioimmunotherapy as a treatment for CD30-positive lymphomas. *J. Nucl. Med.* **2025**, *66* (6), 909.
(45) Kang, Y.-F.; Chen, J.-M.; Xu, B.-C.; Xu, J.-N.; Qin, Q.; Wu, H.-L.; Wang, J.; Wang, R.-K.; Wu, Y.-R.; Tang, W.-J.; Zeng, Y.-C. Calibrating the RT-cGAS-STING axis to drive cold-to-hot tumor transformation: mechanistic foundations and translational strategies for combination with immunotherapy. *Mol. Cancer* **2026**, *25* (1), 103.
(46) Zhang, S.; Liu, C.; Lu, Q.; Liu, W.; Wu, J.; Liu, J.; Tong, L.; Zhao, K.; Hu, Q.; Chen, X.; Li, L.; Song, X.; Wang, F.; Dai, D.; Wang, R.; Hu, K. Fluorination augments tumor engagement and antitumor immunity of a D-peptide-based radiotheranostic agent for combinatorial immune checkpoint blockade therapy. *J. Immunother. Cancer* **2026**, *14* (3), No. e013732.
(47) Giles, J. R.; Ngiow, S. F.; Manne, S.; Baxter, A. E.; Khan, O.; Wang, P.; Staupe, R.; Abdel-Hakeem, M. S.; Huang, H.; Mathew, D.; Painter, M. M.; Wu, J. E.; Huang, Y. J.; Goel, R. R.; Yan, P. K.; Karakousis, G. C.; Xu, X.; Mitchell, T. C.; Huang, A. C.; Wherry, E. J. Shared and distinct biological circuits in effector, memory and exhausted CD8+ T cells revealed by temporal single-cell transcriptomics and epigenetics. *Nat. Immunol.* **2022**, *23* (11), 1600−1613.
(48) Malouli, D.; Tiwary, M.; Gilbride, R. M.; Morrow, D. W.; Hughes, C. M.; Selseth, A.; Penney, T.; Castanha, P.; Wallace, M.; Yeung, Y.; Midgett, M.; Williams, C.; Reed, J.; Yu, Y.; Gao, L.; Yun, G.; Treaster, L.; Laughlin, A.; Lundy, J.; Tisoncik-Go, J.; Whitmore, L. S.; Aye, P. P.; Schiro, F.; Dufour, J. P.; Papen, C. R.; Taher, H.; Picker, L. J.; Früh, K.; Gale, M.; Maness, N. J.; Hansen, S. G.; Barratt-Boyes, S.; Reed, D. S.; Sacha, J. B. Cytomegalovirus vaccine vector-induced effector memory CD4 + T cells protect cynomolgus macaques from lethal aerosolized heterologous avian influenza challenge. *Nat. Commun.* **2024**, *15* (1), 6007.

https://doi.org/10.1021/acs.molpharmaceut.6c00650
Mol. Pharmaceutics 2026, 23, 4311−4321